Anti-phase domains in cubic GaN

Ricarda Maria Kemper,[1,a)] Thorsten Schupp,[1] Maik Häberlen,[1] Thomas Niendorf,[2] Hans-Jürgen Maier,[2] Anja Dempewolf,[3] Frank Bertram,[3] Jürgen Christen,[3] Ronny Kirste,[4] Axel Hoffmann,[4] Jörg Lindner,[1] and Donat Josef As[1]
[1]*University of Paderborn, Department of Physics, Warburger Str. 100, D-33098 Paderborn, Germany*
[2]*University of Paderborn, Lehrstuhl für Werkstoffkunde, Pohlweg 47-49, D-33098 Paderborn, Germany*
[3]*University of Magdeburg, Institut für Festkörperphysik, P.O. Box 4120, D-39016 Magdeburg, Germany*
[4]*Technische Universität Berlin, Institute of Solid State Physics, Hardenbergstr. 36, D-10623 Berlin, Germany*

(Received 10 October 2011; accepted 7 November 2011; published online 22 December 2011)

The existence of anti-phase domains in cubic GaN grown on 3C-SiC/Si (001) substrates by plasma-assisted molecular beam epitaxy is reported. The influence of the 3C-SiC/Si (001) substrate morphology is studied with emphasis on the anti-phase domains (APDs). The GaN nucleation is governed by the APDs of the substrate, resulting in equal plane orientation and the same anti-phase boundaries. The presence of the APDs is independent of the GaN layer thickness. Atomic force microscopy surface analysis indicates lateral growth anisotropy of GaN facets in dependence of the APD orientation. This anisotropy can be linked to Ga and N face types of the {111} planes, similar to observations of anisotropic growth in 3C-SiC. In contrast to 3C-SiC, however, a difference in GaN phase composition for the two types of APDs can be measured by electron backscatter diffraction, μ-Raman and cathodoluminescence spectroscopy. © *2011 American Institute of Physics*. [doi:10.1063/1.3666050]

I. INTRODUCTION

There is great potential in GaN as basis for highly efficient optoelectronic or high-power electronic devices like laser diodes and transistors.[1–3] The wurtzite phase of GaN has piezoelectric polarization fields along the c-axis, leading to a limited performance of optical devices. The cubic phase (c-GaN) on the other hand is free of such effects because of its crystal symmetry. Due to the absence of these fields, the non-polar and semi-polar systems have attracted growing interest in recent years.

One of the key issues in device fabrication of group III-nitrides is the improvement of the structural quality, because defects like dislocations reduce the device performance. In c-GaN the defect density is currently 10^9–10^{10} cm^{-2} and leads to leakage currents.[4] A first step in enhancement of the structural quality can be achieved through the analysis of the fundamental defect formation mechanisms in c-GaN.

For the growth of c-GaN, 3C-SiC films grown epitaxially on Si (001) by metal organic chemical vapor deposition[5] or ion beam synthesis[6] are the substrate of choice. There are three types of basic defects in epitaxial c-GaN thin films grown on 3C-SiC. The first type are misfit dislocations due to relaxation of a pseudomorphically strained thin layer against the substrate. The second type are dislocations originating in the substrate, which extend into the epilayer. The third type are stacking faults (SFs) on {111} planes. A change of the stacking sequence leads to hexagonal inclusions (h-GaN), which act as defects in the crystal symmetry and result in polar faces.

The 3C-SiC substrate exhibits two types of {111} planes, the Si-face type and the perpendicular C-face type. During the nucleation of the 3C-SiC on an elementary Si substrate anti-phase domains (APDs) are formed which can be interpreted as 3C-SiC domains that are rotated by 90° around the [001] axis. Furthermore, the C-face {111} plane has a lower surface energy and thus has a higher growth rate than the Si-face.[7] Therefore, the formation of APDs and a difference in growth rate between the Ga-face and the N-face of the {111} plane in the c-GaN layer can be expected.

We investigate the heteroepitaxial growth of c-GaN by plasma-assisted molecular beam epitaxy (PAMBE) on 3C-SiC/Si (001) under the influence of a given substrate morphology. Scanning electron microscopy (SEM) and atomic force microscopy (AFM) images of the c-GaN provide clear indications of APDs with pronounced boundaries. Elongated facetted micro crystals on the surface of the c-GaN indicate anisotropic growth influenced by the face type of {111} planes. Given that the two types of APDs are interpreted as mere rotations of each other, phase purity or surface roughness should not be influenced by the orientation of the {111} plane faces. However, our results obtained by electron backscatter diffraction (EBSD), cathodoluminescence spectroscopy (CL) and μ-Raman spectroscopy reveal a clear difference in phase composition of the two types of APDs.

II. EXPERIMENTAL

The c-GaN was grown by PAMBE on 3C-SiC/Si (001) substrate.[8] The used substrates consist of 12 μm thick 3C-SiC (001) layers deposited by low-pressure chemical vapor deposition on 500 μm Si (001).[5] The surface of the 3C-SiC was chemo-mechanically polished, leading to a rms

[a)]Author to whom correspondence should be addressed. Electronic mail: rkemper@mail.uni-paderborn.de.

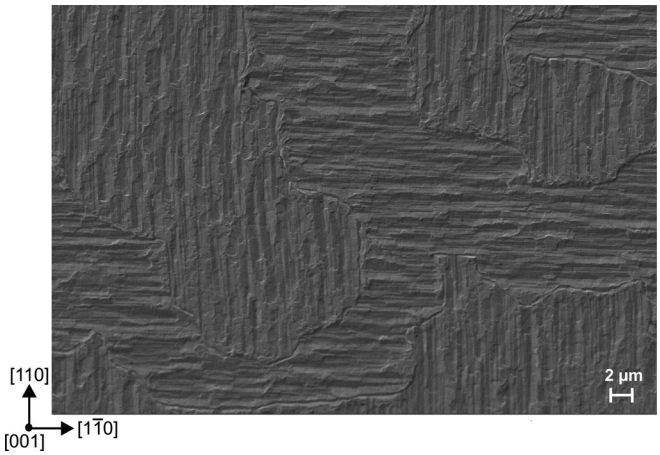

FIG. 1. Top view SEM surface image of sample B. Clearly distinct islands with striations exhibiting perpendicular orientation are an indication of APDs.

roughness of about 1 nm. High-resolution X-ray diffraction (HRXRD) measurements showed a FWHM of the (002) rocking curve of 5 arcmin., indicating a dislocation density of $10^9\,cm^{-2}$. The best growth conditions of c-GaN were achieved under 1 monolayer Ga coverage on the surface and a growth temperature of 740 °C.[9] These conditions were monitored by *in situ* reflection high energy electron diffraction. To facilitate the defect studies, the layer thickness was varied between 450 nm (sample A) and 1.7 μm (sample B).

III. RESULTS AND DISCUSSION

Figure 1 displays an SEM top view surface image of sample B. The surface exhibits surface striations in two perpendicular orientations parallel to [110] and [1$\bar{1}$0], respectively. Regions with striations in either of these directions form islands of arbitrary shape with sizes between 10 to 100 μm. They are considered to be APDs with anti-phase boundaries in between.

To verify the results of the SEM analysis, AFM measurements in contact mode were carried out for sample A and B. The AFM image of sample A is shown in Fig. 2(a). This image reveals two clearly distinguishable domains. In these APDs, the elongated micro crystals have a length of 400–500 nm and exhibit two perpendicular orientations of their facets. Figure 2(b) presents the surface image of sample B showing domain formation as well. The comparison between Fig. 2(a) and Fig. 2(b) reveals that the presence of domains in the c-GaN layer is independent of the layer thickness. However, with increasing layer thickness the length of the elongated micro crystals within the APDs becomes larger to about 1–2 μm in sample B. Consequently the facet formation becomes more pronounced. We conclude an anisotropic lateral growth rate between the APDs in dependence of the polarity of {111} facets. Similar to what has been shown for c-GaN grown by metal organic chemical vapor deposition, the Ga- and N-terminated {111} facets possess different lateral growth rates.[10]

The AFM analysis supports the results of the SEM images and confirms the existence of APDs in c-GaN induced by the substrate. To determine which face type in 3C-SiC induces the face type in c-GaN, we utilize the electronegativity in the Linus Pauling scale as means for the Gibbs free energy. The electronegativities for the involved elements are: Ga 1.81, Si 1.90, C 2.55, and N 3.04.[11] As a result, we conclude the Si-face type {111} planes of the substrate induce Ga-face type {111} planes in the c-GaN and C-face type {111} planes of the substrate induce N-face type {111} planes.

HRXRD allows the investigation of the defect density and phase purity of the c-GaN layer averaged about all domains. Figure 3 shows a HRXRD reciprocal space map of sample B. The content of hexagonal inclusions was determined by the intensity ratio of the c-GaN (002) and h-GaN (10-11) reflections in the reciprocal space map. The hexagonal content increases with the layer thickness from $< 1\%$ in sample A to 15% in sample B. The defect density,[12] determined by the FWHM of the rocking curve of the c-GaN (002) reflection, decreases from $8.4 \cdot 10^9$ cm^{-2} to $4.5 \cdot 10^9$ cm^{-2} with increasing c-GaN layer thickness from 450 nm to 1.7 μm.

In summary, with increasing layer thickness, the three dimensional growth becomes more pronounced and {111} facets are formed, which favor the formation of SFs and hexagonal inclusions. These defects are thermodynamically stable and their amount increases with the c-GaN layer thickness.

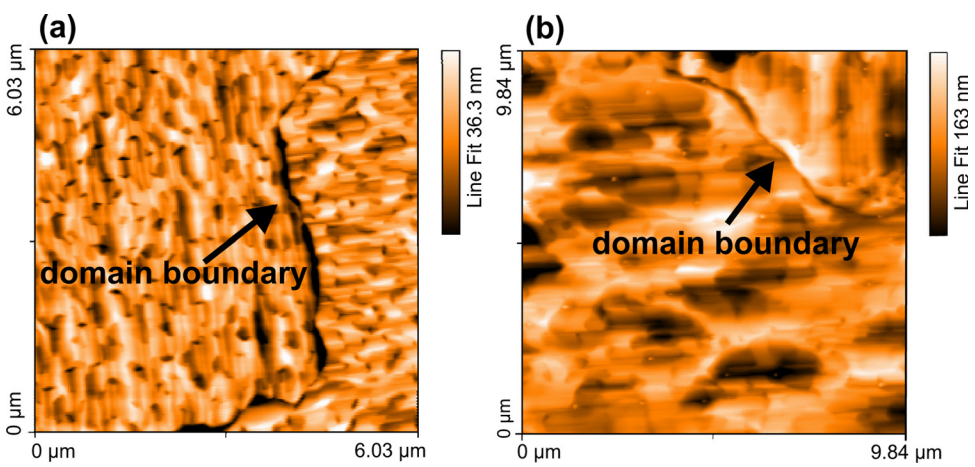

FIG. 2. (Color online) AFM surface images of (a) sample A (450 nm thick c-GaN layer) and (b) sample B (1.7 μm thick c-GaN layer) establish the existence of APDs in c-GaN. The domain formation is independent of the c-GaN layer thickness.

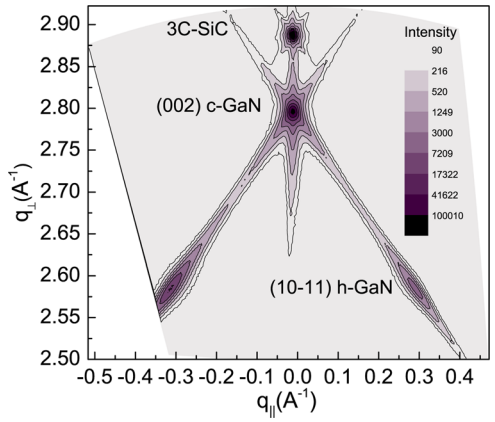

FIG. 3. (Color online) Symmetrical reciprocal space map around the (002) reflection of sample B (1.7 μm thick c-GaN layer).

The phase identification of various APDs of sample B was achieved by EBSD, where Kikuchi diffraction patterns have been correlated to the crystal planes of the sample.[13] Crystal plane identification was achieved by a Hough-transformation of the recorded diffraction patterns followed by a least-square fit to simulated Kikuchi patterns of both the cubic and the hexagonal phase, yielding a phase identification based on the smallest error. The measurement area on the sample surface, which was tilted by about 70° in the measurement setup to increase the signal, is shown in the side view SEM image in Fig. 4. The EBSD data were recorded with a step size of 0.6 μm and an angular resolution of 1–2°. Figure 4 shows the corresponding phase map, where the cubic phase is depicted in red and the hexagonal phase is shown in green.

The comparison between the SEM image of the measurement area and the phase map clearly indicates a different fraction of hexagonal GaN for adjacent domains. For reference, one APD with facet orientation $\perp$ [110] is marked by a white line in the SEM image (Fig. 4). This domain can be identified in the phase map as cubic phase containing hexagonal inclusions. In contrast to this domain, the APDs $\parallel$ [110] have a major fraction of the hexagonal phase. Thus, the defect formation within the ADPs is different and can be allocated to the crystal direction. These results are evidence for the micro crystals within the APDs not being structurally equal and that there is an anisotropic growth of Ga- and N-{111} planes.

Further structural information about the APDs is given by μ-Raman measurements, which were carried out in backscattering z(…)$\underline{z}$ geometry. The 532 nm line of a Nd:YAG-laser with a power of 60 mW was used for excitation. In this configuration, the incident beam of the laser is parallel to the [001] growth direction. For detailed information, line scans with a lateral resolution of 0.25 μm in a measurement area of (20 μm× 20 μm) have been executed.

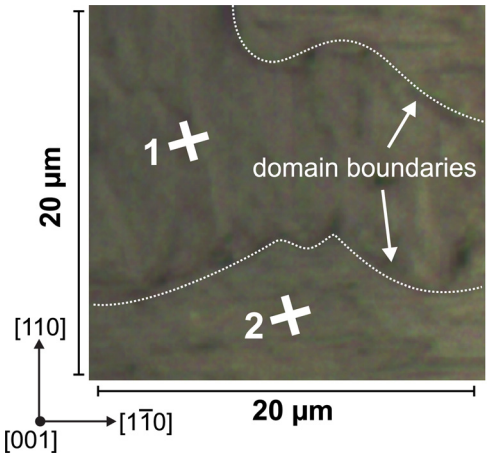

FIG. 5. (Color online) Optical image of the (20 μm×20 μm) μ-Raman measurement area of sample B. Position 1 and 2 mark the measurement area of the μ-Raman spectra 1 and 2 in Fig. 6 in adjacent APDs.

Figure 5 shows a top view optical image of the measurement area with two adjacent domains of sample B. Two typical Raman spectra, taken at room temperature at the position 1 and 2 marked by crosses in Fig. 5, are shown in Fig. 6. The blue curve (position 1) mainly presents a spectrum of the hexagonal content in the c-GaN with a dominating E_2(high) mode at 565 cm^{-1}.[14] The small FWHM of about 4.3 cm^{-1} indicates a low defect density in the hexagonal phase. The observation of the transversal optical (TO) component of the A_1 mode at 538 cm^{-1} provides an indication of a tilted c-axis.

In the cubic spectrum (red curve, position 2), the TO and the longitudinal optical (LO) modes are located at 551 cm^{-1} and 735 cm^{-1}. These values can be compared to the literature value of c-GaN grown on GaAs.[14] The c-axis of the cubic phase is nearly parallel to the incident laser beam and the intensity ratio of the LO mode and the TO mode indicates a correlation between the c-axis of the cubic and the hexagonal GaN. Additionally, the Raman shift of the hexagonal E_2 mode and the cubic TO mode in the spectra reveals that both phases are tensile strained.

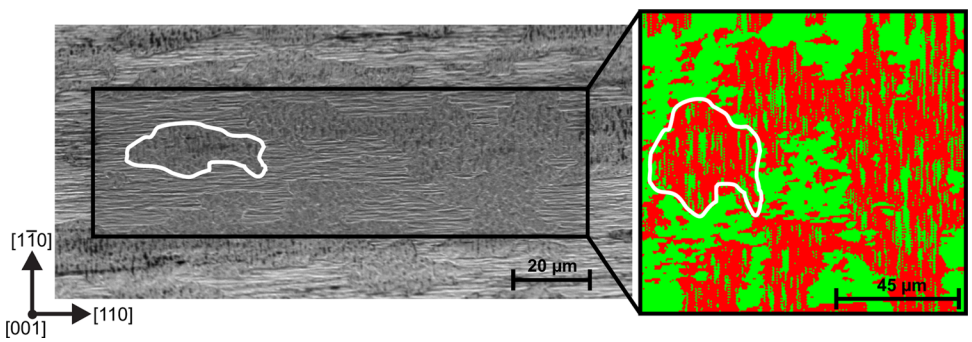

FIG. 4. (Color online) Left: Tilted view (~70°) SEM image of the EBSD measurement area on the surface of sample B. Right: Phase map showing regions of predominantly cubic (dark, red) and hexagonal (bright, green) GaN. The APD $\perp$ [110] marked by a white line in the SEM image, can be identified in the phase map as cubic phase containing hexagonal inclusions.

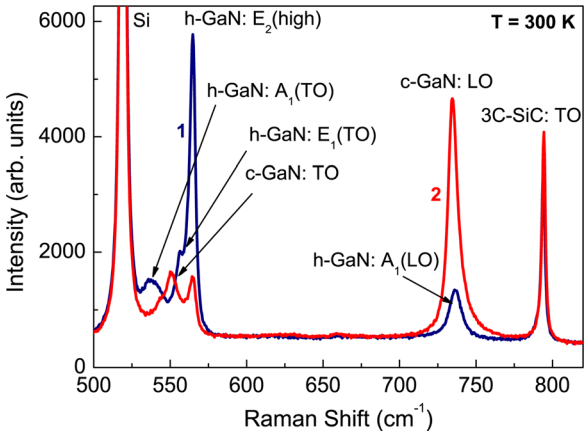

FIG. 6. (Color online) Two typical μ-Raman spectra (1 and 2) at room temperature taken from the measurement area in Fig. 5.

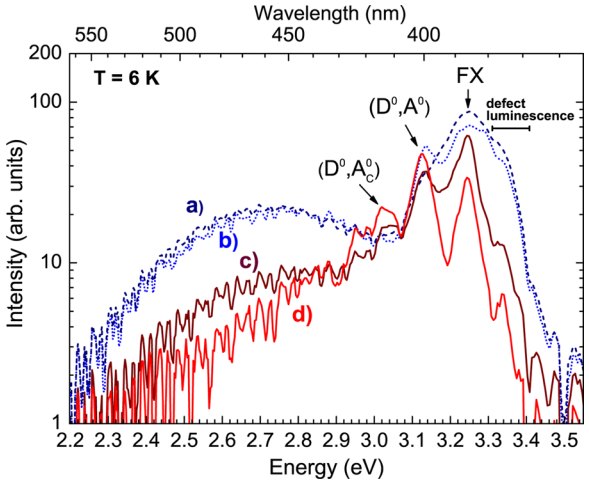

FIG. 8. (Color online) Local low-temperature CL spectra of APDs of sample B. The corresponding measurement areas of the CL emission spectra are marked in the SEM image in Fig. 9(a). Spectra a) and b) (dashed lines) are taken from measurement areas located in an APD ∥ [110] and the measurement areas of the emission spectra c) and d) (solid lines) are positioned in the adjacent APD ⊥ [110].

Figure 7(a) presents a plot of the position of the cubic TO mode and the TO component of the hexagonal E_1 mode. A correlation between the image of the measurement area (Fig. 5) and the plotted data affirm the dominance of the cubic phase in the APD ⊥ [110] and the dominant presence of the hexagonal phase in the APD ∥ [110]. These results are in good agreement with the observations made by EBSD.

In addition, the map shows streaks related to the cubic phase along the [010] direction in the APD ∥ [110]. The reason for this streaky pattern can be found in the detailed analysis of the substrate. Figure 7(b) shows a map of the Raman shift of the 3C-SiC TO mode at 794 cm^{-1} (see Ref. 15), also exhibiting a streaky pattern. Thus, the substrate does not only transfer the APDs into the c-GaN layer, but also the local strain fields seemingly influence the growth of c-GaN in the APDs.

The optical properties of the APDs were recorded spatially resolved by low-temperature (6 K) CL measurements. In a dedicated SEM, the electron beam was scanned over the area of interest (256 × 200 pixels). A complete luminescence spectrum was taken from each pixel with an acceleration voltage of 10 kV and a beam current of 1.3 nA.[16,17]

Figure 8 shows local CL emission spectra of sample B. The corresponding measurement areas are marked in the SEM image in Fig. 9(a). The CL emission spectra a) and b) (dashed lines) are taken from measurement areas located in an APD ∥ [110] and the measurement areas of the emission spectra c) and d) (solid lines) are positioned in the adjacent APD ⊥ [110]. The corresponding CL emission spectra shown in Fig. 8 contain four dominant peaks. The peak at 3.25 eV is due to the radiative recombination of the free exciton (FX) in cubic GaN.[18] Additionally there is a donor-acceptor (D^0, A^0) pair recombination peak at 3.14 eV, a C-related donor-acceptor transition (D^0, A_C^0) at 3.04 eV and a deep compensating complex in the range from 2.2–2.9 eV.[19] Furthermore, there is an interesting emission line at 3.33 eV, which is assigned to defect luminescence related to the hexagonal phase. In comparison, the local CL spectra between the APDs significantly differ from each other, because the spectra a) and b), marked in dashed lines, show more intensity of the hexagonal defect luminescence at 3.33 eV and a pronounced defect luminescence in the range of 2.2–2.9 eV. This indicates a different defect density in adjacent domains.

Figure 9(a) shows the SEM image of the whole (70 μm × 50 μm) CL measurement area with a matching CL wavelength map (Fig. 9(b)). The CL wavelength image (CLWI) displays the emission wavelength of the local maximum CL intensity of each pixel.[16] The color distribution of this map reproduces the sample morphology (Fig. 9(a)) showing APDs. The APDs ⊥ [110] contain, on average, more regions dominated by luminescence of the donor-acceptor pair recombination around 3.14 eV than APDs ∥ [110]. In addition, these domains show a smaller amount of

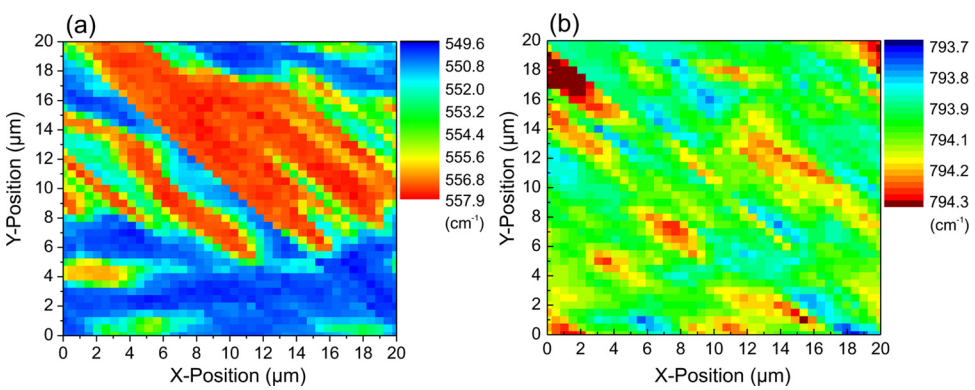

FIG. 7. (Color online) (a) Map of the position of the cubic TO mode and the hexagonal E_1 component of the TO mode (cm^{-1}), (b) μ-Raman map of the Raman shift of the TO mode (cm^{-1}) of the 3C-SiC substrate.

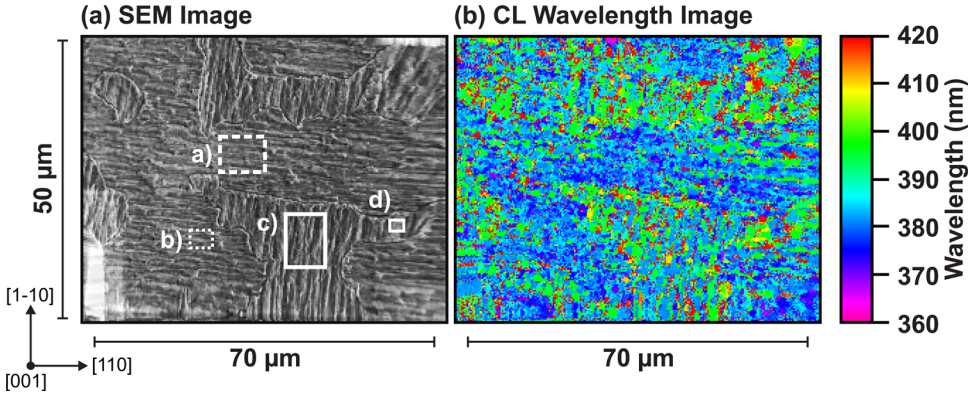

FIG. 9. (Color online) SEM image (a) of the whole ($70\,\mu m \times 50\,\mu m$) CL-measurement area with matching CL wavelength image (b) of sample B. The marked measurement areas a), b), c) and d) in the SEM image correspond to the CL emission spectra in Fig. 8.

areas with dominant defect luminescence around 3.33 eV than the adjacent domains. The CLWI measurements agree well with the EBSD measurements showing that APDs ∥ [110] contain a higher fraction of defects than APDs ⊥ [110].

IV. CONCLUSION

It is shown that cubic GaN grown on 3C-SiC/Si (001) by MBE forms APDs which are induced by the substrate and oriented with their facets parallel or perpendicular to the [110] direction. Several independent measurement techniques like EBSD, μ-Raman and CL demonstrate the formation of hexagonal inclusions preferentially in one type of the APDs. Since according to HRXRD measurements the hexagonal fraction of GaN increases with increasing layer thickness along with the increasing formation of surface facets, it is concluded that the presence of {111} facets plays an important role in the formation of hexagonal inclusions. For one direction, the {111} facets are N- terminated, while for the other they are Ga- terminated. As it is known that c-GaN growth requires Ga rich conditions, it is assumed that hexagonal inclusions form preferentially on the N- terminated facets. Micro-Raman measurements indicate an additional influence of the 3C-SiC substrate: Local strain fields are extending through the 3C-SiC into the c-GaN layer and affect the growth of the cubic or the hexagonal phase. In order to develop effective defect reduction methods, further studies will try to elucidate the influence of the different facet types and strain on extended defect formation. These studies may help to improve the structural quality of existing electrical and optoelectronical devices based on cubic GaN grown on 3C-SiC (001).

ACKNOWLEDGMENTS

The authors would like to thank Prof. Dr. W. Bremser and especially Dipl.-Chem. Ing. N. Buitkamp (University of Paderborn) for access to the SEM. The work at Paderborn was financially supported by German Science Foundation (DFG) (Project No. AS 107/4-1, SCHM 136/11-1 and GRK 1464). The work at TU-Berlin was supported by DFG via SFB 787.

[1]S. Nakamura, I. Mukai, and M. Senoh, Appl. Phys. Lett. **64**, 1687 (1994).
[2]S. Rajan, P. Waltereit, C. Poblenz, S. J. Heikman, D. S. Green, J. S. Speck, and U.K. Mishra, IEEE Electron Device Lett. **25**, 247 (2004).
[3]H. Machhadani, M. Tchernycheva, S. Sakr, L. Rigutti, R. Colombelli, E. Warde, C. Mietze, D. J. As, and F. H. Julien, Phys. Rev. B **83**, 075313 (2011).
[4]E. Tschumak, R. Granzer, J. K. N. Lindner, F. Schweiz, K. Lischka, H. Nagasawa, M. Abe, and D. J. As, Appl. Phys. Lett. **96**, 253501 (2010).
[5]T. Chassagne, A. Leycuras, C. Balloud, P. Arcade, H. Peyre, and S. Juillaguet, Materials Science Forum **457–460**, 273 (2004).
[6]M. Häberlen, J. W. Gerlach, B. Murphy, J. K. N. Lindner, and B. Stritzker, J. Cryst. Growth **312**, 762 (2010).
[7]H. Nagasawa, M. Abe, K. Yagi, T. Kawahara, and N. Hatta, Phys. Status Solidi B **245**(7), 1272 (2008).
[8]D. J. As, T. Frey, D. Schikora, K. Lischka, V. Cimalla, J. Pezoldt, R. Goldhahn, S. Kaiser, and W. Gebhardt, Appl. Phys. Lett. **76**, 1686 (2000).
[9]J. Schörmann, S. Potthast, D. J. As, and K. Lischka, Appl. Phys. Lett. **90**, 041918 (2009).
[10]Y. Fu, H. Yang, D. G. Zhao, X. H. Zheng, S. F. Li, Y. P. Sun, Z. H. Feng, Y. T. Wang and L. H. Duan, J. Cryst. Growth **225**, 45 (2001).
[11]D. R. Lide, CRC *Handbook of Chemistry* and *Physics*: A *Ready*-Reference *Book of Chemical and Physical Data*, 90th ed, (CRC Taylor & Francis, Boca Raton, Fl., 2009), pp. 9–98.
[12]P. Gay, P. B. Hirsch, and A. Kelly, Acta Metall. **1**, 315 (1953).
[13]L. Reimer, *Scanning Electron Microscopy*, 2nd ed, (Springer, New York, 1998), pp. 368–374.
[14]H. Siegle, L. Eckey, A. Hoffmann, C. Thomson, B. K. Meyer, D. Schikora, M. Hankeln, and K. Lischka, Solid State Commun. **96**(12), 943 (1995).
[15]Z. C. Feng, C. C. Tin, R. Hu, and J. Williams, Thin Solid Films **266**, 1 (1995).
[16]J. Christen, M. Grundmann, and D. Bimberg, J. Vac. Sci. Technol. B **9**, 2358 (1991).
[17]F. Bertram, T. Riemann, J. Christen, A. Kaschner, A. Hoffmann, C. Thompsen, K. Hiramatsu, T. Shibata, and N. Sawaki, Appl. Phys. Lett. **74**, 359 (1999).
[18]D. J. As, F. Schmilgus, C. Wang, B. Schöttker, D. Schikora, and K. Lischka, Appl. Phys. Lett. **70**, 1311 (1997).
[19]D. J. As and U. Köhler, J. Phys.: Condens. Matter **13**, 8923(2001).